

Unbiased Correction Relations for Galaxy Cluster properties Derived from *Chandra* and *XMM-Newton*

Hai-Hui Zhao, Cheng-Kui Li, Yong Chen, Shu-Mei Jia, Li-Ming Song

ABSTRACT

We use a sample of 62 clusters of galaxies to investigate the discrepancies of gas temperature and total mass within r_{500} between *XMM-Newton* and *Chandra* data. Comparisons of the properties show that (1) Both the de-projected and projected temperatures determined by *Chandra* are higher than those of *XMM-Newton* and there is a good linear relation for the de-projected temperature: $T_{Chandra}=1.25 \times T_{XMM}-0.13$. (2) The *Chandra* mass is much higher than *XMM-Newton* mass with a bias of 0.15 and our mass relation is: $\log_{10} M_{Chandra}=1.02 \times \log_{10} M_{XMM}+0.15$. To explore the reasons for the discrepancy in mass, we recalculate the *Chandra* mass (expressed as $M_{Ch}^{mo/d}$) by modifying its temperature with the de-projected temperature relation. The results show that $M_{Ch}^{mo/d}$ is more close to the *XMM-Newton* mass with the bias reducing to 0.02. Moreover, $M_{Ch}^{mo/d}$ are corrected with the r_{500} measured by *XMM-Newton* and the intrinsic scatter is significantly improved with the value reducing from 0.20 to 0.12. These mean that the temperature bias may be the main factor causing the mass bias. At last, we find that $M_{Ch}^{mo/d}$ is consistent with the corresponding *XMM-Newton* mass derived directly from our mass relation at a given *Chandra* mass. Thus, the de-projected temperature and mass relations can provide unbiased corrections for galaxy cluster properties derived from *Chandra* and *XMM-Newton*.

Subject headings: galaxies: clusters: general — X-rays: galaxies: clusters — intra-cluster medium

1. Introduction

Galaxy clusters are the most massive gravitationally bound objects in the Universe, and they can provide crucial information for studies of large scale-structure (Bahcall 1988; Zhang et al. 2006; Willis et al. 2013) and tracing cosmic evolution (Allen et al. 2011). The cluster mass is

Particle Astrophysics Division, Institute of High Energy Physics, Chinese Academy of Sciences, Beijing 100049; zhaohh@ihep.ac.cn

probably the most interesting global parameter for characterizing a galaxy cluster (Böhringer et al. 2004). The cluster mass function, which is sensitive to cosmological parameters, can give observational constraints to cosmology (Vikhlinin et al. 2009, Tinker et al. 2012). Precise mass estimate strongly depends on the measurement of gas temperature in the cluster. By accurately measuring temperatures and masses of galaxy clusters in a large sample, one can calibrate the mass-temperature relation, which is widely used to improve the accuracy of the cosmological parameters determination (Nevalainen et al. 2010).

Precise properties of galaxy cluster can be derived from *XMM-Newton* and *Chandra*, which have high spatial resolution and large field of view. However, there are discrepancies in the measurements of gas temperature and total mass between the two instruments. Typically, the *Chandra* temperature is 5%-15% higher than the value of *XMM-Newton* (Kotov & Vikhlinin 2005; Vikhlinin et al. 2005; Snowden et al. 2008; Reese et al. 2010). The total mass within r_{2500} derived from *Chandra* was roughly 15% higher than that from *XMM-Newton* (Mahdavi et al. 2013).

Many works have attempted to modify the systematic differences in the cluster’s temperature or mass between these two instruments. By multiplying the effective area of *Chandra*/ACIS with the corresponding splines of the stacked residuals, Schellenberger et al. (2014) changed the energy dependence of effective area and found that the temperatures between *Chandra*/ACIS and *XMM-Newton*/pn were consistent. Li et al. (2012) tried to fit *Chandra* spectra with *XMM-Newton* temperatures and presented that the modified *Chandra* mass of Abell 1835 was consistent with the *XMM-Newton* mass. These works focused on looking for the reasons of discrepancy in temperature or mass, but they didn’t give an correction relation which can be used directly in combining *Chandra* and *XMM-Newton* data to build a large sample.

In this work, we use a sample of 62 clusters of galaxies to study the discrepancies of temperature and mass derived from *Chandra* and *XMM-Newton*, aiming to find good correction methods for the discrepancies of properties. This paper is organized as follows. Section 2 shows the reduction procedures for *Chandra* and *XMM-Newton* data and the methods to obtain temperature profile and total mass. The relations of temperature and mass between the two instruments are listed in section 3. In Section 4, we attempt to illustrate the temperature bias is the main factor causing the mass discrepancy. We prove our mass relation between the two instruments is robust to correct the *Chandra* mass, which can bring the masses obtained with *Chandra* and *XMM-Newton* into consistency in Section 5. We draw our conclusions in Section 6. Throughout this paper, the selected energy band is 0.5-7.0 keV and a flat Λ CDM cosmological model is used with $\Omega_M = 0.3$, $\Omega_\Lambda = 0.7$ and $H_0 = 70 \text{ km s}^{-1} \text{ Mpc}^{-1}$.

2. Sample Selection and Data Analysis

Using a flux-limited ($f \geq 1.0 \times 10^{-11} \text{ erg s}^{-1} \text{ cm}^2$) method, we have built a large cluster sample from the RASS (Grandi et al. 1999), HIFLUGCS (Thomas et al. 2002), REFLEX (Böhringer et al. 2004), NORAS (Böhringer et al. 2000), XBACs (Ebeling et al. 1996) and BCS (Ebeling et al. 1998) catalogs. In this sample, there are 72 clusters observed by both *Chandra* and *XMM-Newton*. We analyze all of the clusters to find the overall biases of cluster properties between the two instruments. Data reduction procedures for *Chandra* and *XMM-Newton* are as follows.

The *XMM-Newton* data are processed with Science Analysis System (SAS) 12.6.0. In this paper, we consider the pn/EPIC data which have larger effective area. The observations are taken in Extended Full Frame mode or Full Frame mode. The events with FLAG = 0, PATTERN ≤ 4 are used, the read out of time and the vignetting effects are also corrected. Since the X-ray flux of the cluster should be stable during the observation period, we discard all the intervals with prominent flares and then select only those intervals with count rates within 3σ of the residual average value. After the removal of the prominent background flares and point sources, the observation of ‘Lockman Hole’ (observation ID: 0147511801, hereafter LH) is used to subtract the background. Considering the background difference between the LH and the source, we use the local background to monitor the residual background. The data reduction procedures for *XMM-Newton* can be referred to Zhao et al. (2013).

The *Chandra* data are performed by CIAO 4.3 and CALDB 4.4.0. We analyze the *Chandra* data following the method discussed in Li et al. (2012). The tool LC_CLEAN in CIAO is used to scan the light curve of data for flares, and the Good Time Intervals (GTIs) are selected. The prominent background flares are removed as in *XMM-Newton*. We extract background from the standard set of CTI-corrected ACIS blank sky in the *Chandra* CALDB (Markevitch et al. 2003) and the process is the same as *XMM-Newton*.

For both *XMM-Newton* and *Chandra* data, a double-background subtraction method is applied to correct the Particle background and Cosmic X-ray Background as used in Jia et al. (2004, 2006). Assuming spherical symmetry, the spectra are extracted from annular regions centered on the X-ray emission peak. The criterion of ~ 2000 net counts in 2-7 keV band per bin is used to determine the width of each ring (Zhang et al. 2006, 2007). The minimum width of the rings are set at $0.5'$ or $0.25'$ for *XMM-Newton*/EPIC or *Chandra*/ACIS, respectively. It is wide enough for us to ignore the Point Spread Function (PSF) effect. The de-projected spectrum of each shell is derived by subtracting all the contributions from the outer regions (see Chen et al. 2003, 2007 and Jia et al. 2004, 2006 for detailed calculation).

2.1. De-projected Temperature Profile and Total Mass

The spectral analysis is carried out using XSPEC version 12.8.1. The plasma emission model Mekal (Mewe et al. 1985) and WABS model (Morrisson & McCammon 1983) are used to fit the de-projected spectra and then the de-projected temperature, metallicity and normalizing constant $norm$ in each ring can be obtained. We fit the radial de-projected temperature profile by the following equation (Xue et al. 2004):

$$T(r) = T_0 + \frac{A}{r/r_0} \exp\left(-\frac{(\ln r - \ln r_0)^2}{\omega}\right), \quad (1)$$

where T_0 , A , r_0 , and ω are free parameters.

For the electron density profile, we divide the cluster into several annular regions (10-30 regions, depending on count rate of the cluster) centered on the emission peak. Then, the de-projected photon counts in each shell are obtained. Since the de-projected temperature and abundance profiles are known, we can simulate the spectrum of each shell in XSPEC. By fitting the simulative spectra, $norm$ of each shell are determined, which can provide the corresponding electron density n_e (Jia et al. 2006). A double- β model is adopted to fit the de-projected electron density profile (Chen et al. 2003):

$$n_e(r) = n_{01}\left[1 + \left(\frac{r}{r_{c1}}\right)^2\right]^{-\frac{3}{2}\beta_1} + n_{02}\left[1 + \left(\frac{r}{r_{c2}}\right)^2\right]^{-\frac{3}{2}\beta_2}, \quad (2)$$

where n_{01} and n_{02} are electron number density parameters, β_1 and β_2 are the slope parameters, and r_{c1} and r_{c2} are the core radii of the inner and outer components, respectively. Then, with the assumptions of hydrostatic equilibrium and spherical symmetry, the gravitational mass of cluster within radius r can be determined as (Fabricant et al. 1980):

$$M(< r) = -\frac{k_B T r^2}{G \mu m_p} \left[\frac{d(\ln n_e)}{dr} + \frac{d(\ln T)}{dr} \right]. \quad (3)$$

where μ is the mean molecular weight of gas and the value is assumed to 0.62. k_B is the Boltzman constant, m_p is the proton mass, and G is the gravitational constant. Hereafter, $M_{Chandra}$ and M_{XMM} represent the original *Chandra* and *XMM-Newton* mass within r_{500} , in which the mean gravitational mass density is equal to 500 times the critical density at the cluster redshift. The primary parameters of all 62 galaxy clusters are given in Table 1.

2.2. Statistical Analysis

In the following, we investigate the temperature and mass relationships between *Chandra* and *XMM-Newton* data. The commonly used BCES Bisector method (Akritas & Bershady 1996) is used to fit the relations. We perform the relations of temperature and mass in the form:

$$Y = B \times X + A, \quad (4)$$

where A and B are the two free parameters to be estimated, X and Y represent the temperatures (T_i) or the logarithmic values of masses ($\log_{10} M_i$) derived from *XMM-Newton* and *Chandra*. The intrinsic scatter around the best-fit relation is calculated as (Morandi et al. 2007; Pratt et al. 2009):

$$S = \left[\sum_i w_i ((Y_i - B \times X_i - A)^2 - \sigma_{Y_i}^2) / (N - 2) \right]^{1/2}, \quad (5)$$

where

$$w_i = \frac{1/\sigma_i^2}{(1/N) \sum_{i=1}^N 1/\sigma_i^2}, \quad \sigma_i^2 = \sigma_{Y_i}^2 + B^2 \sigma_{X_i}^2, \quad (6)$$

N is the total number of data, σ_{Y_i} and σ_{X_i} are the statistical errors of the measurements Y_i and X_i , respectively.

In order to evaluate the systematic deviation, we define the bias of temperature or mass measurement as the average vertical distance between the best-fit line and the line of $Y=X$ ($bias = \frac{1}{N} \sum (Y_i - X_i)$). The results of fits for all the relations are given in Table 3.

3. The Relations of Properties between *Chandra* and *XMM-Newton*

3.1. The Relations of Temperatures Determined by *Chandra* and *XMM-Newton*

For each cluster, the de-projected temperatures are obtained in several rings. To avoid the effects of cool cores and keep the qualities of spectral data, we derive the global temperatures by the volume average of the de-projected temperatures, which is in the radii of $0.15\text{-}0.5r_{500}$ (Vikhlinin et al. 2009) and $0.2\text{-}0.5r_{500}$ (Zhang et al. 2008) for *Chandra* and *XMM-Newton* data, respectively. Due to the effects of PSF, a larger inner boundary of $0.2r_{500}$ is set for *XMM-Newton* data. The maximum radii (R_{max}), out to which the temperature profiles can reach for each cluster as a fraction of r_{500} , are calculated. We list the global temperatures and R_{max} in Table 1. The extended temperature and electron density profiles may introduce some uncertainties to the cluster mass. Ten clusters (e.g., 2A0335, A1060, A262), whose r_{500} are much larger than the field of view (the R_{max} is smaller than $0.5r_{500}$), are not considered in the following analysis. Comparing the global temperatures between the two instruments, the de-projected temperature derived from *Chandra* is higher than that of *XMM-Newton* by about 1.24 keV as shown in the left panel of Fig. 1. There is

a good linear relation for the de-projected temperatures measured by the two instruments and the best-fit relation is $T_{Chandra}=1.25\times T_{XMM}-0.13$ with the intrinsic scatter of 0.50.

In order to find the discrepancy of temperatures between *Chandra* and *XMM-Newton* directly, we extra the projected spectra within two fixed rings (the radii are 1.0'-2.5' and 2.5'-4.0') and get the projected temperatures for each cluster. The comparison of projected temperatures between the two instruments is shown in the right panel of Fig. 1. There still exist a linear relation between the two temperatures and the relation is $T_{Chandra}=1.30\times T_{XMM}-0.83$ with the intrinsic scatter of 0.57. The projected temperature obtained with *Chandra* is higher than that of *XMM-Newton* by about 0.79 keV, which is smaller than the bias of de-projected temperature. Our discrepancy (11%) of the projected temperatures is consistent with the value of 10-15% in Nevalainen et al. (2010).

3.2. The Relation of Masses Derived from *Chandra* and *XMM-Newton*

Using the radial de-projected temperature and intra-cluster medium density distributions, we obtain the total mass within r_{500} for both *Chandra* and *XMM-Newton*. Comparison of the total masses between the two instruments is shown in Fig. 2. There is a logarithmic relationship for the masses between the two instruments: $\log_{10} M_{Chandra}=1.02 \times \log_{10} M_{XMM}+0.15$, and the intrinsic scatter around the this relation is 0.19. Fixing the slope of our mass relation to 1.0, we find that the mass determined by *Chandra* is higher about 36% that that of *XMM-Newton*. Using our definition of bias in Section 2.2, the bias between the two masses is 0.15. We also obtain the total mass within r_{2500} for both *Chandra* and *XMM-Newton* and find a difference of about 20% which is larger than the result of 15% for 19 clusters in Mahdavi et al. (2013).

4. The Effects of Temperature on Mass Discrepancy

The results above indicate that both the temperature and mass derived from *Chandra* are higher than the values obtained with *XMM-Newton*. It is interesting to test whether the discrepancy in mass is caused by temperature. Many recent works reveal that the properties derived from *XMM-Newton* are more reliable (Böhringer et al. 2004; Zhang et al. 2010; Li et al. 2012), and we try to modify the *Chandra* mass with the relations of temperatures in this paper. Using the relations of temperatures between the two instruments, we correct the *Chandra* temperature of each ring and the corrected temperature profiles for *Chandra* data are obtained. Based on the modified *Chandra* temperature, we recover the electron density distribution. Then, we get the amended *Chandra* masses ($M_{Ch}^{mo/d}$ and $M_{Ch}^{mo/p}$ for the *Chandra* mass modified by the de-projected and projected temperature relations, respectively). We compare the modified *Chandra* masses with the M_{XMM}

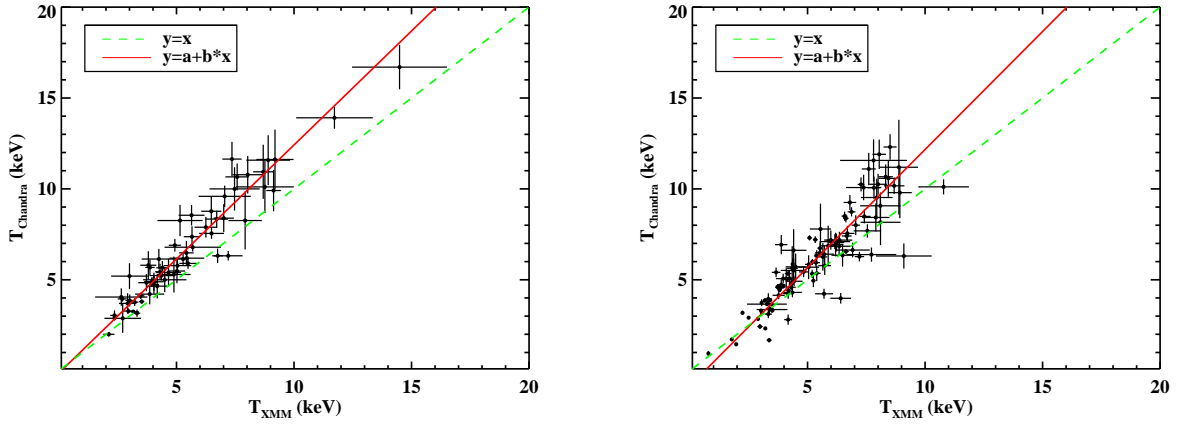


Fig. 1.— Left panel: comparison of global temperatures determined by *Chandra* and *XMM-Newton*. The global temperatures are the volume averages of the de-projected temperatures which are limited to the ranges of $0.15\text{--}0.5\ r_{500}$ and $0.2\text{--}0.5\ r_{500}$ for T_{Chandra} and T_{XMM} , respectively; Right panel: comparison of *Chandra* and *XMM-Newton* projected temperatures. For each cluster, we derive two projected temperatures within fixed rings (the radii are $1.0'\text{--}2.5'$ and $2.5'\text{--}4.0'$). The red lines show the best-fit temperature relations, while the green dashed lines show the relations of $Y=X$.

as shown in Fig. 3. Our results show that both the modified *Chandra* masses are more close to the M_{XMM} , the bias between M_{XMM} and $M_{Ch}^{mo/d}$ is 0.02 while the bias between M_{XMM} and $M_{Ch}^{mo/p}$ is 0.08. Compared with the bias of 0.15 in Section 3.2, the mass bias is almost resolved by the temperature correction, this means the temperature may be the main factor causing the mass bias.

After correcting the *Chandra* mass, the bias of mass between the two instruments is indeed smaller than before, but the intrinsic scatters are not improved as shown in Table 3. In the mass comparisons above, the masses derived from different instruments are integrated within their own r_{500} , and different r_{500} may also bring bias to the mass determination. To reduce such discrepancy, we recalculate the *Chandra* mass with the r_{500} measured by *XMM-Newton* (the modified *Chandra* masses are expressed as $M_{Ch}^{mo/d,r}$ and $M_{Ch}^{mo/p,r}$). The comparisons of M_{XMM} with $M_{Ch}^{mo/d,r}$ and $M_{Ch}^{mo/p,r}$ are shown in Fig. 4 and the results are listed in Table 3. There are obvious improvements in the intrinsic scatters: the intrinsic scatter is reduced from 0.20 to 0.12 for the M_{XMM} - $M_{Ch}^{mo/d,r}$ relation; and the value change from 0.18 to 0.11 for the M_{XMM} - $M_{Ch}^{mo/p,r}$ relation. The $M_{Ch}^{mo/d,r}$ is still in agreement with M_{XMM} with the bias of 0.03 ± 0.01 , while the $M_{Ch}^{mo/p,r}$ is higher than M_{XMM} with the bias of 0.08 ± 0.01 as shown in Fig. 4. This reveals that the corrected method using the de-projected temperature relation is more effective. Thus, after correcting the temperature and r_{500} , the intrinsic scatter is smaller than before and the $M_{Ch}^{mo/d,r}$ is consistent with M_{XMM} .

5. Comparison of Methods for Correcting *Chandra* Mass

We have obtained the *Chandra* masses, $M_{Ch}^{mo/d}$, modified by the relation of de-projected temperatures derived from *Chandra* and *XMM-Newton*. In the calculating process of $M_{Ch}^{mo/d}$, we need to modify the *Chandra* temperature and the *Chandra* electron density based on the modified temperature. In addition, we can directly get the corresponding *XMM-Newton* mass (expressed as M_{Ch}^{mo}) from our mass relation in Section 3.2 at given *Chandra* mass. Both the methods can give the corrected *Chandra* masses and we compare them in Fig. 5 to find whether the *Chandra* masses modified by the two methods are consistent. The result shows that M_{Ch}^{mo} is in good agreement with $M_{Ch}^{mo/d}$ and the scatter around the best-fit relation is 0.09. It means that the *Chandra* mass corrected by our mass relation directly is consistent with that corrected by the complex de-projected temperature calculation. Thus, our mass relation is robust to correct the *Chandra* mass and the relations of de-projected temperature and mass can provide unbiased correction for the cluster properties measured by the two instrument. Moreover, based on the correction of the de-projected temperature, we can obtain some detailed information for clusters, e.g., the distribution of mass, the gas fraction and entropy.

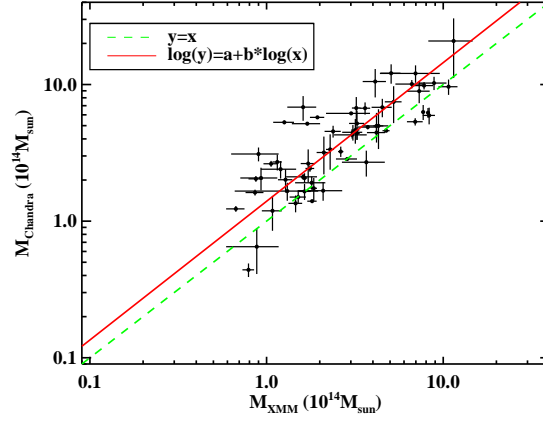


Fig. 2.— Comparison of original de-projected masses obtained with *Chandra* and *XMM-Newton*.

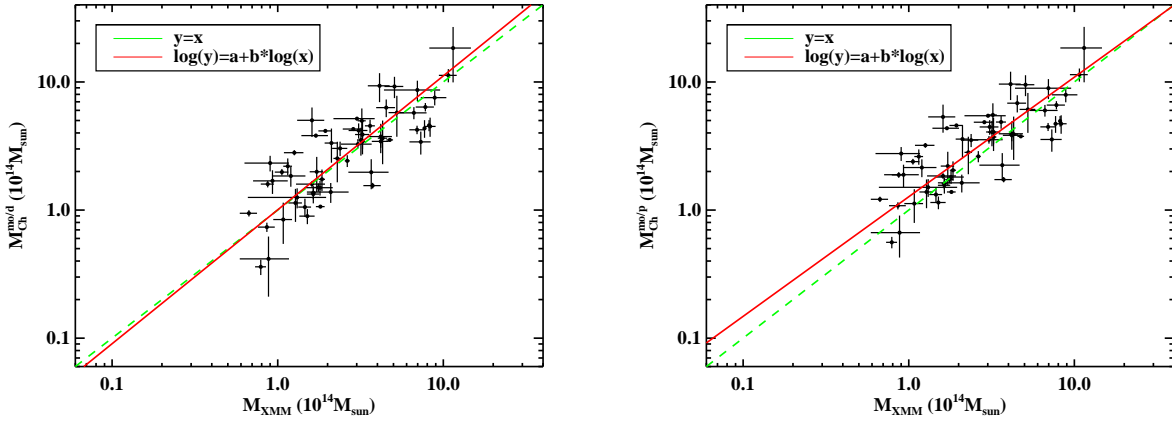


Fig. 3.— Comparison of *XMM-Newton* and corrected *Chandra* masses. Left panel: the *Chandra* masses are modified by the relation of de-projected temperatures; Right panel: the *Chandra* masses are modified by the relation of projected temperatures.

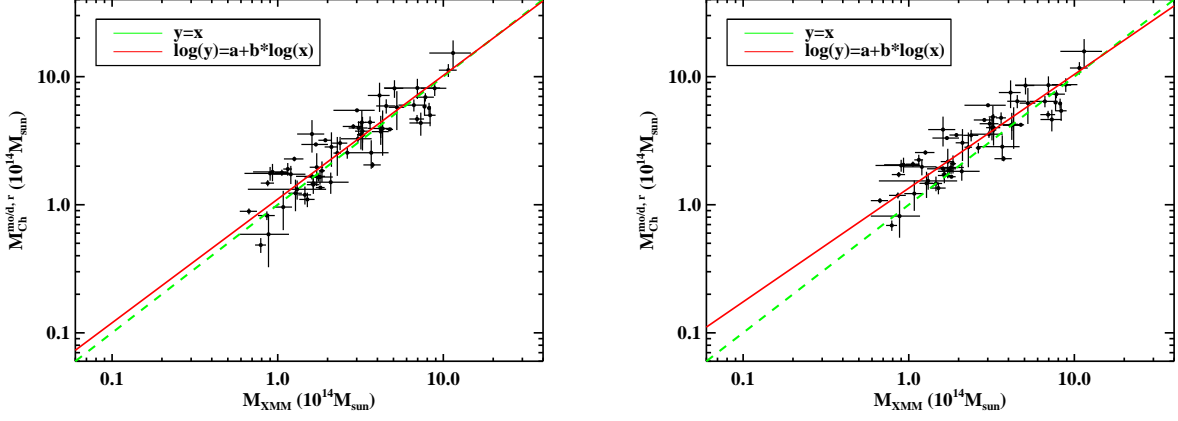


Fig. 4.— Same as Fig. 3, excepting that the corrected *Chandra* masses are integrated to the r_{500} measured by *XMM-Newton*.

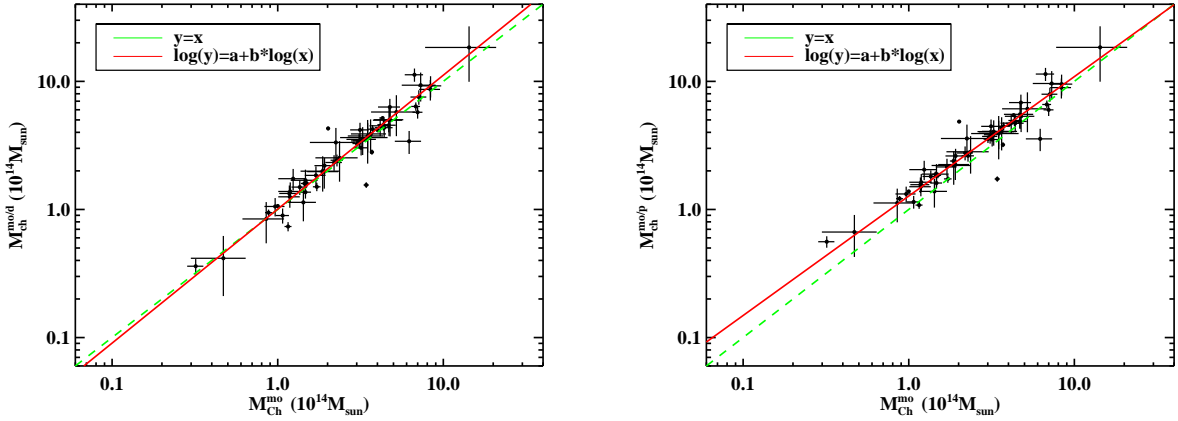


Fig. 5.— Comparisons of *Chandra* masses modified by temperature relations and by our mass relation in Section 3.2.

6. Conclusion

We use a sample of 62 galaxy clusters to study the discrepancies of temperature and mass within r_{500} between *XMM-Newton* and *Chandra* data. Using the same analysis procedure, we obtain gas temperatures and total masses for each cluster with two instruments. Comparisons of gas temperature and mass show that: (1) The temperatures derived from *Chandra* are higher than those of *XMM-Newton* and there is a good linear relation for the de-projected temperature relation: $T_{Chandra}=1.25 \times T_{XMM}-0.13$. (2) The *Chandra* mass overestimates 36% than the value of *XMM-Newton* and the relation is $\log_{10} M_{Chandra}=1.02 \times \log_{10} M_{XMM}+0.15$.

To look for the possible causes of mass discrepancy, we recalculate the *Chandra* mass with the de-projected and projected temperature relation (expressed as $M_{Ch}^{mo/d}$ and $M_{Ch}^{mo/p}$), respectively. The results reveal that $M_{Ch}^{mo/d}$ is more close to the M_{XMM} with the bias of only 0.02. Moreover, the *Chandra* masses are recalculated with the r_{500} measured by *XMM-Newton* and the intrinsic scatter is significantly improved with the value reducing from 0.20 to 0.12. Thus, the mass discrepancy is almost resolved by the temperature correction, and the temperature bias may be the main factor causing the mass bias. At last, we find that $M_{Ch}^{mo/d}$ is consistent with the corrected *Chandra* mass which is directly modified by our mass relation. So, the de-projected temperature and original mass relation can give the unbiased corrections for galaxy cluster properties derived from *Chandra* and *XMM-Newton*. These relations are robust to combine *Chandra* and *XMM-Newton* data into a large unbiased cluster sample.

This research was supported by the National Natural Science Foundation of China under grants Nos. 11103022, and by the Strategic Priority Research Program on Space Science, the Chinese Academy of Sciences, grant No. XDA04010300.

REFERENCES

- Akritas, M. G., & Bershad, M. A. 1996, *ApJ*, 470, 706
- Allen, S. W., Evrard, A. E., & Mantz, A. B. 2011, *ARA&A*, 49, 409
- Bahcall N. A. 1988, *ARA&A*, 26, 631
- Böhringer, H., Voges, W., Huchra, J. P., et al. 2000, *ApJ*, 129, 435
- Böhringer, H., Schuecker, P., Guzzo, L., et al. 2004, *A&A*, 425, 367
- Chen, Y., Ikebe, Y., & Böhringer, H. 2003, *A&A*, 407, 41
- Chen, Y., Reiprich, T. H., Böhringer, H., et al. 2007, *A&A*, 466, 805

Table 1: observations and cluster properties.

Name	redshift	N_H (10^{20}cm^{-2})	$T_{Chandra}$ (keV)	$M_{Chandra}$ ($10^{14}M_\odot$)	T_{XMM} (keV)	M_{XMM} ($10^{14}M_\odot$)	R_{max} (r_{500})
A119	0.044	3.1	6.14 ± 0.56	5.29 ± 0.16	4.25 ± 0.73	1.26 ± 0.17	0.69
A133	0.057	1.6	4.89 ± 0.50	2.70 ± 0.58	4.04 ± 0.42	3.67 ± 1.00	0.68
A1413	0.143	1.6	8.39 ± 0.77	5.34 ± 0.33	7.01 ± 0.43	6.94 ± 0.71	1.29
A1644	0.047	5.3	5.00 ± 0.68	1.67 ± 0.26	4.50 ± 0.92	2.09 ± 0.59	0.94
A1650	0.085	1.5	5.90 ± 0.30	4.41 ± 0.47	5.49 ± 0.37	3.25 ± 0.13	1.17
A1651	0.085	1.7	6.48 ± 0.65	6.73 ± 1.37	5.42 ± 0.31	3.22 ± 0.18	0.94
A1689	0.183	0.18	10.94 ± 1.49	10.25 ± 1.14	8.69 ± 0.43	8.87 ± 1.56	1.48
A1750	0.085	2.5	4.65 ± 0.67	2.07 ± 0.39	4.18 ± 0.44	0.93 ± 0.22	1.86
A1795	0.062	1.2	6.32 ± 0.40	6.29 ± 0.79	6.75 ± 0.23	7.70 ± 0.18	0.57
A1835	0.252	2.2	10.66 ± 0.74	10.08 ± 0.71	7.58 ± 0.50	6.64 ± 1.28	2.14
A1914	0.171	1	10.78 ± 1.03	6.81 ± 1.05	8.03 ± 0.65	4.52 ± 0.59	1.74
A2029	0.077	3.2	8.34 ± 0.46	4.47 ± 0.58	6.71 ± 0.48	3.08 ± 0.40	1.13
A2034	0.113	1.5	7.55 ± 0.30	2.85 ± 0.08	6.49 ± 0.53	2.86 ± 0.39	1.40
A2052	0.035	2.9	3.25 ± 0.09	1.62 ± 0.08	3.16 ± 0.23	0.86 ± 0.10	0.76
A2063	0.036	2.9	5.20 ± 0.71	2.04 ± 0.10	3.00 ± 0.78	0.87 ± 0.08	0.83
A2065	0.072	2.8	5.48 ± 0.67	3.35 ± 0.97	5.02 ± 0.34	2.29 ± 0.12	0.66
A2142	0.089	4.1	9.59 ± 0.59	10.52 ± 2.47	7.05 ± 1.11	4.12 ± 0.62	0.99
A2147	0.035	3.29	4.05 ± 0.48	1.66 ± 0.25	2.65 ± 1.11	1.31 ± 0.65	0.82
A2163	0.203	12.3	16.70 ± 1.22	20.83 ± 9.67	14.49 ± 2.02	11.45 ± 3.22	0.90
A2199	0.03	0.8	4.87 ± 0.22	2.07 ± 0.17	3.94 ± 0.20	1.64 ± 0.06	0.69
A2204	0.151	5.9	10.11 ± 1.44	5.94 ± 0.83	8.76 ± 1.23	8.32 ± 0.66	1.28
A2219	0.228	1.7	11.62 ± 1.64	9.82 ± 0.61	9.19 ± 0.79	7.79 ± 0.98	2.37
A2255	0.081	2.5	6.79 ± 0.24	6.15 ± 0.14	5.69 ± 1.20	3.01 ± 0.84	1.39
A2256	0.058	4	5.80 ± 0.77	4.54 ± 0.45	3.80 ± 0.34	2.38 ± 0.25	0.88
A2319	0.056	8.77	9.91 ± 1.14	6.22 ± 0.51	9.13 ± 0.31	8.20 ± 0.14	0.70
A2390	0.233	10.7	13.91 ± 0.60	9.64 ± 1.24	11.72 ± 1.63	10.72 ± 1.32	1.70
A2589	0.042	4.39	3.77 ± 0.21	1.35 ± 0.19	3.22 ± 0.16	1.46 ± 0.13	0.69
A2597	0.085	2.5	3.95 ± 0.16	2.71 ± 0.36	2.69 ± 0.19	1.15 ± 0.07	1.46
A2626	0.057	92	3.16 ± 0.20	1.40 ± 0.03	3.32 ± 0.14	1.81 ± 0.11	0.85
A2657	0.04	5.3	4.21 ± 0.56	2.11 ± 0.10	3.86 ± 0.62	1.61 ± 0.32	0.76
A3112	0.075	2.5	5.44 ± 0.44	4.64 ± 0.95	4.30 ± 0.21	3.18 ± 0.17	1.10
A3128	0.062	1.5	3.70 ± 0.56	3.10 ± 0.36	2.92 ± 0.37	0.90 ± 0.27	1.30
A3158	0.059	1.1	5.66 ± 0.37	5.75 ± 0.15	4.40 ± 0.26	1.94 ± 0.18	1.03
A3266	0.059	1.5	10.00 ± 1.19	8.94 ± 1.64	7.47 ± 1.07	7.31 ± 1.07	0.76
A3391	0.051	5.4	6.19 ± 0.29	4.88 ± 0.18	5.44 ± 0.74	3.74 ± 0.45	0.95
A3528	0.054	6.2	5.29 ± 0.99	6.83 ± 1.40	4.89 ± 0.71	1.61 ± 0.30	1.00
A3532	0.055	6	5.40 ± 0.75	2.40 ± 0.35	4.66 ± 0.53	1.20 ± 0.27	1.31
A3558B	0.048	3.6	5.78 ± 0.45	5.17 ± 0.14	5.04 ± 0.59	1.70 ± 0.31	0.61
A3562	0.049	3.9	4.74 ± 0.51	2.43 ± 0.13	4.04 ± 0.21	1.76 ± 0.10	1.03

Table 1. continued.

Name	redshfit	N_H (10^{20}cm^{-2})	$T_{Chandra}$ (keV)	$M_{Chandra}$ ($10^{14}M_\odot$)	T_{XMM} (keV)	M_{XMM} ($10^{14}M_\odot$)	R_{max} (r_{500})
A3571	0.039	3.9	8.55 ± 0.56	5.19 ± 1.26	5.64 ± 0.55	3.25 ± 0.32	0.58
A3581	0.023	4.3	2.00 ± 0.13	0.44 ± 0.05	2.12 ± 0.24	0.79 ± 0.06	0.56
A3667	0.056	4.6	6.90 ± 0.35	4.59 ± 0.10	4.93 ± 0.26	4.75 ± 0.22	0.83
A3827	0.098	2.8	7.89 ± 0.57	4.98 ± 1.61	6.25 ± 0.48	4.30 ± 0.28	1.10
A399	0.072	10.6	8.26 ± 0.86	4.28 ± 0.26	5.15 ± 0.96	3.05 ± 0.64	0.92
A4059	0.048	3.27	4.88 ± 0.27	1.65 ± 0.22	3.96 ± 0.25	1.64 ± 0.14	0.81
A478	0.088	15.3	6.32 ± 0.26	4.45 ± 0.41	7.20 ± 0.61	4.19 ± 0.49	0.98
A496	0.033	5.7	5.68 ± 0.43	3.18 ± 0.98	3.87 ± 0.20	2.11 ± 0.19	0.96
A576	0.038	5.7	4.84 ± 0.47	2.63 ± 0.13	3.72 ± 0.35	1.06 ± 0.10	0.96
A754	0.054	4.6	11.58 ± 1.37	12.06 ± 1.76	8.90 ± 0.93	6.97 ± 2.59	0.57
A85	0.06	3.6	6.14 ± 0.32	3.23 ± 0.28	5.28 ± 0.22	2.63 ± 0.09	0.70
EXO0422	0.039	6.4	3.86 ± 0.33	2.01 ± 0.39	3.01 ± 0.18	1.28 ± 0.12	0.69
HERCULES	0.037	3.4	2.88 ± 0.80	0.65 ± 0.24	2.71 ± 0.78	0.88 ± 0.29	0.73
HydraA	0.054	4.9	3.80 ± 0.11	1.74 ± 0.33	3.52 ± 0.11	1.85 ± 0.08	0.81
IIIZW54	0.031	16.68	3.04 ± 0.28	1.19 ± 0.34	2.36 ± 0.18	1.08 ± 0.14	0.68
MKW3s	0.044	3.2	4.12 ± 0.18	1.91 ± 0.21	3.48 ± 0.15	1.80 ± 0.35	0.68
MKW8	0.026	2.6	3.28 ± 0.14	1.23 ± 0.06	2.95 ± 0.27	0.67 ± 0.08	0.71
PKS0745	0.103	43.49	8.77 ± 0.79	6.71 ± 0.69	6.48 ± 0.43	3.61 ± 0.25	1.19
RXCJ1504.1-0248	0.215	6	11.64 ± 0.95	12.10 ± 1.96	7.36 ± 0.41	5.07 ± 0.66	2.04
RXCJ1558.3-1410	0.097	11.1	5.23 ± 0.27	2.64 ± 0.71	4.36 ± 0.51	1.72 ± 0.16	1.71
RXCJ1720.1+2637	0.164	3.9	8.26 ± 1.59	7.47 ± 2.25	7.92 ± 0.71	5.24 ± 0.57	1.60
RXCJ2014.8-2430	0.16	13.22	7.37 ± 0.57	4.98 ± 1.22	5.66 ± 0.35	4.19 ± 0.70	1.70
S1101	0.056	1.9	2.89 ± 0.11	1.50 ± 0.14	2.36 ± 0.06	1.51 ± 0.16	0.91
2A0335	0.035	18.6	3.86 ± 0.25	1.43 ± 0.04	4.03 ± 0.80	2.96 ± 0.44	0.45
A1060	0.013	4.9	4.33 ± 1.25	1.24 ± 0.28	3.15 ± 0.25	0.93 ± 0.06	0.34
A262	0.016	5.5	2.84 ± 0.12	0.80 ± 0.05	2.48 ± 0.33	0.58 ± 0.07	0.37
A3526	0.011	8.2	3.09 ± 0.16	0.82 ± 0.03	3.19 ± 0.21	1.10 ± 0.06	0.29
AWM7	0.017	9.21	4.25 ± 0.39	1.42 ± 0.19	3.59 ± 0.57	1.31 ± 0.15	0.36
COMA	0.023	0.9	8.97 ± 0.19	8.45 ± 0.30	7.14 ± 0.47	8.89 ± 1.15	0.29
MKW4	0.02	1.9	1.81 ± 0.10	0.56 ± 0.07	2.04 ± 0.29	0.62 ± 0.12	0.44
NGC1550	0.013	11.6	1.68 ± 0.25	0.55 ± 0.09	1.44 ± 0.06	0.25 ± 0.01	0.47
NGC5813	0.007	4.2	0.72 ± 0.14	0.11 ± 0.01	0.75 ± 0.01	0.17 ± 0.02	0.23
OPHIUCHUS	0.028	20.14	8.42 ± 0.17	3.97 ± 0.18	8.65 ± 0.38	12.50 ± 0.30	0.45

Notes. The redshfits of clusters used in this sample are quoted from NASA/IPAC Extragalactic Database (NED). The hydrogen absorption columns, N_H , are obtained from Dickey & Lockman (1990). r_{500} are measured by *XMM-Newton*. $T_{Chandra}$ and T_{XMM} are the global temperatures defined in Section 3.1, $M_{Chandra}$ and M_{XMM} represent the original *Chandra* and *XMM-Newton* masses within their own r_{500} . R_{max} is the maximum radius, out to which the temperature profile can reach for each cluster as a fraction of r_{500} . Ten clusters, which R_{max} are smaller than $0.5r_{500}$, are listed in the end of table.

Table 2: Comparisons of parameters derived from *Chandra* and *XMM-Newton*.

	A	B	intrinsic scatter	bias
$T_{XMM}-T_{Chandra}$ (dep)	-0.13 ± 0.26	1.25 ± 0.07	0.50 ± 0.02	1.24 ± 0.07
$T_{XMM}-T_{Chandra}$ (p)	-0.83 ± 0.32	1.30 ± 0.08	0.57 ± 0.01	0.79 ± 0.05
$M_{XMM}-M_{Chandra}$	0.15 ± 0.05	1.02 ± 0.09	0.19 ± 0.01	0.15 ± 0.01
$M_{XMM}-M_{Ch}^{mo/d}$	0.01 ± 0.05	1.05 ± 0.08	0.20 ± 0.01	0.02 ± 0.01
$M_{XMM}-M_{Ch}^{mo/p}$	0.10 ± 0.04	0.93 ± 0.07	0.18 ± 0.01	0.08 ± 0.01
$M_{XMM}-M_{Ch}^{mo/d,r}$	0.04 ± 0.03	0.97 ± 0.06	0.12 ± 0.01	0.03 ± 0.01
$M_{XMM}-M_{Ch}^{mo/p,r}$	0.13 ± 0.03	0.89 ± 0.06	0.11 ± 0.01	0.08 ± 0.01
$M_{Ch}^{mo}-M_{Ch}^{mo/d}$	0.01 ± 0.02	1.05 ± 0.03	0.09 ± 0.01	0.02 ± 0.01
$M_{Ch}^{mo}-M_{Ch}^{mo/p}$	0.10 ± 0.02	0.93 ± 0.04	0.09 ± 0.01	0.08 ± 0.01

Note. dep: the temperatures in the relation are de-projected temperatures. p: the temperatures are projected temperature. M_{XMM} and $M_{Chandra}$ represent the original de-projected masses determined by *Chandra* and *XMM-Newton*, respectively. $M_{ch}^{mo/d}$ and $M_{ch}^{mo/p}$ are the *Chandra* masses modified by the de-projected and projected temperature relations, respectively. $M_{ch}^{mo/d,r}$: the $M_{ch}^{mo/d}$ is recalculated with the r_{500} measured by *XMM-Newton*. $M_{ch}^{mo/p,r}$: the $M_{ch}^{mo/p}$ is recalculated with the r_{500} measured by *XMM-Newton*. The M_{Ch}^{mo} is derived from the relation of $M_{XMM}-M_{Chandra}$ at given $M_{Chandra}$. A linear fitting, $Y=B \times X+A$, is used for the temperature relations. We perform the mass relations with logarithmic values of the parameters in the form: $\log_{10}Y=B \times \log_{10}X+A$. The bias represents the systematic deviation in temperature or mass measurement between different instruments. The relations which can provide unbiased corrections for the properties measured by *Chandra* and *XMM-Newton* are highlighted with bold letters.

- Dickey, J. M., & Lockman, F. J. 1990, ARA&A, 28, 215
- Ebeling, H., Voges, W., Böhringer, H., et al. 1996, MNRAS, 281, 799
- Ebeling, H., Edge, A. C., Böhringer, H., et al. 1998, MNRAS, 301, 881
- Fabricant, D., Lecar, M., & Gorenstein, P. 1980, ApJ, 241, 552
- Grandi, S. D., Böhringer, H., Guzzo, L., et al. 1999, ApJ, 514, 148
- Jia, S. M., Chen, Y., Lu, F. J., et al. 2004, A&A, 423, 65
- Jia, S. M., Chen, Y., & Chen, L. 2006, ChJAA, Vol. 6, 181
- Kotov, O., & Vikhlinin, A. 2005, ApJ, 633, 781
- Li, C. K., Jia, S. M., Chen, Y., et al. 2012, A&A, 545, A100
- Mahdavi, A., Hoekstra, H., Babul, A., et al. 2013, ApJ, 767, 116
- Markevitch, M., Bauz, M. W., Biller, B., et al. 2003, ApJ, 583, 70
- Mewe, R., Gronenschild, E. H. B. M., & Van den Oord, G. H. J. 1985, A&AS, 62, 197
- Morandi, A., Ettori, S., & Moscardini, L. 2007, MNRAS, 379, 518
- Morrison, R., & McCammon, D. 1983, ApJ, 270, 119
- Nevalainen, J., David, L., & Guainazzi, M. 2010, A&A, 523, A22
- Pratt, G. W., Croston, J. H., Arnaud, M., et al. 2009, A&A, 498, 361
- Reese, E. D., Kawahara, H., Kitayama, T., et al. 2010, ApJ, 721, 653
- Schellenberger, G., Reiprich, T. H., Lovisari, L., et al. 2014, submitted (arXiv:1404.7130v1)
- Snowden, S. L., Mushotzky, R. F., Kuntz, K. D., & Davis, D. S. 2008, A&A, 478, 615
- Tinker, J. L., Sheldon, E. S., Wechsler, R. H., et al. 2012, ApJ, 745, 16
- Thomas, H. R., Böhringer, H., 2002, ApJ, 567, 716
- Vikhlinin, A., Markevitch, M., Murray, S. S., Jones, C., et al. 2005, ApJ, 628, 655
- Vikhlinin, A., Kravtsov, A. V., Burenin, R. A., et al. 2009, ApJ, 692, 1060
- Willis J. P., Clerc, N., Bremer, M. N., et al. 2013, MNRAS, 430, 134

- Xue, Y. J., Böhringer, H., & Matsushita, K., 2004, A&A, 420, 833
- Zhao, H. H., Jia, S. M., Chen, Y., et al. 2013, ApJ, 778, 124
- Zhang, Y. Y., Böhringer, H., Finoguenov, A., et al. 2006, A&A, 456, 55
- Zhang, Y. Y., Finoguenov, A., Böhringer, H., et al. 2007, A&A, 467, 437
- Zhang, Y. Y., Finoguenov, A., Böhringer, H., et al. 2008, A&A, 482, 451
- Zhang, Y. Y., Okabe, N., Finoguenov, A., et al. 2010, ApJ, 711, 1033